12. Study on Fast Fracture and Crack Arrest

Takeshi KANAZAWA *, *Member*, Susumu MACHIDA *, *Member*,
Tokuo TERAMOTO *, *Member* and Hitoshi YOSHINARI *, *Member*

(From J.S.N.A. Japan, Vol. 141, June 1977, Vol. 142, Dec. 1977 and Vol. 144, Dec. 1978)

Summary

Since the experimentally proven inadequacy of static approximation to fast fracture and crack arrest was brought to light, a lot of structural engineers and researchers are interested in dynamic aspects of fast fracture and crack arrest.

This paper gives firstly some numerical results obtained with the use of finite difference method to show its usefulness as a tool to analyze dynamic fracture mechanics problems. The results of numerical computation compare well with the corresponding analytically solved solutions in terms of stress, strain and energy flow.

Then the experimental results of brittle crack propagation and arrest on structural steels are analyzed using finite difference method. The material toughness against fast fracture is defined as a function of temperature and crack velocity. Using the thus defined fracture toughness, crack propagating behaviors are predicted through numerical simulations for some limited cases. This implies a possibility to develop simple methods for crack arrester design.

1. Introduction

Arrest of a fast moving crack is of interest not only from a scientific but also from an engineering point of view. Particularly in designing large weld structures, steel components and weldments with moderate levels of notch toughness together with appropriate combinations of crack arresters are used to prevent extensive and catastrophic failures of the structure. Current ship construction rules, for instance, lists material specifications for steels used as crack arresters, but the level of toughness requirement is rather arbitrarily specified on an empirical basis.

For relatively short arrested crack, static approximation using linear fracture mechanics concept or arrest toughness concept has yielded useful results for theoretical interpretations and design applications of brittle fracture propagation and arrest tests currently in use. Later experimental investigations using very wide specimens, however, have revealed that the above simple interpretation is inconsistent with the experimental results involving long arrested cracks. The experimentally proven inadequacy of the static approximation has resulted in a renewed concern today over the theoretical basis for an engineering criterion for arrest of a fast moving crack.

In order to seek a more reasonable theory of fast fracture and crack arrest and to study the extent which dynamical aspects affects the interpretation of results of unstable, fast crack propagation arrest tests as well as the philosophy of crack design, the authors initiated a dynamic fracture mechanics analysis of crack propagation

* University of Tokyo

and arrest with the use of a finite difference method.

Results of a numerical experiment are presented, and experimental results for structural steels are analyzed and discussed in terms of dynamic fracture mechanics analysis with a focus on energetic aspect of the crack propagation processes.

2. Numerical Analysis of Fast Moving Crack Using Finite Difference Method

In order to discuss the fast crack propagation such as brittle fracture, a consideration of dynamic effects on mechanical aspects are indispensable. Some theoretical analyses of fast and steadily moving crack in an infinite plate have been available,[1),2),3)] but analyses on a crack propagating in a finite body particularly non-steady crack propagation including crack arrest, are quite limited. These are so complicated that quantitative analysis is almost impossible without recourse to numerical technique. Numerical methods are useful, because of being able to deal with arbitrary geometrical and mechanical boundary conditions even if they are time dependent.

This followings give some results of numerical experiments on dynamic crack propagation in two dimensional elastic body using finite difference method. The conventional equations of motion for infinitesimal strain theory of elasticity in plane strain state are solved numerically. Calibrating computation of the coded computer program based on the finite difference technique was run for a running crack which is analytically solved by Broberg[3)] and the results were found to compare very well each other except the strain and stress values in the vicinity of the crack tip.

2.1 *Equations of Motion*

The equations of motion in a two dimensional elastic body are represented as follows:

$$\rho\frac{\partial^2 u}{\partial t^2}=\frac{\partial \sigma_x}{\partial x}+\frac{\partial \tau_{xy}}{\partial y}$$

$$\rho\frac{\partial^2 v}{\partial t^2}=\frac{\partial \tau_{xy}}{\partial x}+\frac{\partial \sigma_y}{\partial y} \qquad (1)$$

where ρ is specific density, and u and v are the displacements in x and y directions, respectively. The elastic constitutive equations are given by

$$\sigma_x=(\lambda+\mu)\frac{\partial u}{\partial x}+\lambda\frac{\partial v}{\partial y}$$

$$\sigma_y=\lambda\frac{\partial u}{\partial x}+(\lambda+\mu)\frac{\partial v}{\partial y}$$

$$\tau_{xy}=\mu\left(\frac{\partial v}{\partial x}+\frac{\partial u}{\partial y}\right) \qquad (2)$$

where λ and μ are the Lame's constants. By substituting eq. (2) into eq. (1), we have

$$\frac{\partial^2 u}{\partial t^2}=C_1{}^2\frac{\partial^2 u}{\partial x^2}+(C_1{}^2-C_2{}^2)\frac{\partial^2 v}{\partial x\partial y}+C_2{}^2\frac{\partial^2 u}{\partial y^2}$$

$$\frac{\partial^2 v}{\partial t^2}=C_2{}^2\frac{\partial^2 v}{\partial x^2}+(C_1{}^2-C_2{}^2)\frac{\partial^2 u}{\partial x\partial y}+C_1{}^2\frac{\partial^2 v}{\partial y^2} \qquad (3)$$

where

$C_1=\{(\lambda+2\mu)/\rho\}^{1/2}$: velocity of longitudinal stress wave

$C_2=(\mu/\rho)^{1/2}$: velocity of transvers stress wave

Equations (3) were solved taking the x-axis along the crak line with the origin at the center of a crack.

Two techniques, that is, explicit and implicit method, are available to solve the finite difference equations corresponding to eq. (3). The former is easier to be solved but the solution may diverge unless time increment Δt was taken appropriately small enough. The latter, on the other hand, require larger computation time but gives stable and more accurate solutions. If a relevant time and geometrical increments are adopted the results by the both methods agree well each other. In this paper the explicit method is adopted to save computer time with careful choice of time and spatial increments.

A plate ($2B \times 2H$) containing a crack is divided by lattice with the mesh size of $h \times h$. From eq. (3) the displacement u and v at the nodal point (x,y) and at the time $(t+\Delta t)$ are formulated as follows:

$$\begin{aligned}
u(x, y, t+\Delta t) &= 2u(x, y, t) - u(x, y, t-\Delta t) \\
&+ \left(\frac{C_1 \Delta t}{h}\right)^2 \{u(x+h, y, t) - 2u(x, y, t) \\
&+ u(x-h, y, t)\} + \frac{1}{4}\left(\frac{C_1 \Delta t}{h}\right)^2 \left\{1 - \left(\frac{C_2}{C_1}\right)^2\right\} \\
&\times \{v(x+h, y+h, t) - v(x+h, y-h, t) \\
&- v(x-h, y+h, t) + v(x-h, y-h, t)\} \\
&+ \left(\frac{C_2 \Delta t}{h}\right)^2 \{u(x, y+h, t) - 2u(x, y, t) \\
&+ u(x, y-h, t)\} \\
v(x, y, t+\Delta t) &= 2v(x, y, t) - v(x, y, t-\Delta t) \\
&+ \left(\frac{C_2 \Delta t}{h}\right)^2 \{v(x+h, y, t) - 2v(x, y, t) \\
&+ v(x-h, y, t)\} + \frac{1}{4}\left(\frac{C_1 \Delta t}{h}\right)^2 \left\{1 - \left(\frac{C_2}{C_1}\right)^2\right\} \\
&\times \{u(x+h, y+h, t) - u(x+h, y-h, t) \\
&- u(x-h, y+h, t) + u(x-h, y-h, t)\} \\
&+ \left(\frac{C_1 \Delta t}{h}\right)^2 \{v(x, y+h, t) - 2v(x, y, t) \\
&+ v(x, y-h, t)\} \qquad (4)
\end{aligned}$$

The displacement u, v at the time $(t+\Delta t)$ are obtained from the known values of those at the time $(t-\Delta t)$ and t. Thus value of acceleration is assumed to be a constant value during the period from $(t-\Delta t)$ to $(t+\Delta t)$. The time increment Δt is chosen to satisfy the inequality $(C_1 \Delta t/h) < 1$ on the basis of theory of stability in numerical iteration. Shmuely et al.[4] reported that $(C_1 \Delta t/h)$ should be less than 0.86 for the solution to converge for the Poisson's ratio ν of 0.25, but the upper bound of $(C_1 \Delta t/h)$ might be increased with higher value of ν In this paper, $(C_1 \Delta t/h)$ =0.5 and ν=0.3 are adopted.

2.2 *Some Numerical Examples*

2.2.1 *A crack suddenly formed under uniform tension*

The variation of the normal stress distribution ahead of the crack is examined when a crack of length $2a=11h$ opens up suddenly in a plate ($2B \times 2H$, $B=H=50h$) subjected to a uniform vertical tensile stress σ_0. The solution of this problem is obtained by the superposition of case (a): a crack in a plate is suddenly subjected to crack opening pressure σ_0, and case (b): the plate containing no crack is under uniform tensile stress σ_0. The stresses in the vicinity of the crack tend to approach those values for an infinite body until the stress waves reflected from the boundary reaches the crack tip region. The location of the crack tip is assumed the center of the square mesh. The boundary conditions are

$$\begin{array}{llll}
\sigma_y = -\sigma_0, \ \tau_{xy}=0 & |x| \leq a & \text{and} & y=0 \\
v=0, \ \tau_{xy}=0 & a \leq |x| \leq B & \text{and} & y=0 \\
u=0, \ \tau_{xy}=0 & x=0 & \text{and} & 0 \leq |y| \leq H \\
\sigma_x=0, \ \tau_{xy}=0 & x=B & \text{and} & 0 \leq |y| \leq H \\
\sigma_y=0, \ \tau_{xy}=0 & |x| \leq B & \text{and} & |y|=H
\end{array} \qquad (5)$$

The displacements are normalized as given by

$$U = \frac{\rho C_1^2}{\sigma_0} \frac{u}{h}, \qquad V = \frac{\rho C_1^2}{\sigma_0} \frac{v}{h}$$

Figure 1 shows time variation of dimensionless normal stress in the y-direction

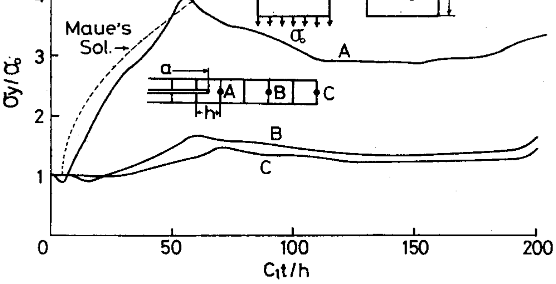

Fig. 1 Time variation of dimensionless stress at three fixed points ahead of a crack

σ_y at three fixed points A, B and C ahead of a crack which are shown in the inset of Fig. 1. The dashed line is the analytical solution for a corresponding problem in an infinite body obtained by Maue[5]. The time dependence of the stress σ_y in the vicinity of the crack tip is given as

$$\frac{\sigma_y}{\sigma_0}=\frac{\sqrt{2(1-2\nu)}}{\pi(1+\nu)}\sqrt{\frac{C_1 t}{r}} \tag{6}$$

where r is the distance of the point considered from the crack tip. The difference between numerical and analytical solutions is probably attributable to the ambiguity in defining crack tip position in finite difference computation and also to relatively large size of the mesh h as compared with crack size a. But the observed difference seems to be small enough from the engineering point of view.

From Fig. 1 it appears that after stress waves pass through the points under consideration, stresses at these points seem to attain the steady value until the arrival of reflected waves from the free boundary of the plate. The steady values of stresses at various points and crack opening displacement attained at the period of $C_1 t/h$ =150 after sudden application of pressure are compared with those for corresponding static case as shown in Figs. 2 and 3, respectively. Figure 2 shows the stress distribution in the vicinity of the crack tip along the lines I (y=0), II (y=h/2), III (y=3h/2). The numerical solution seems to agree well with the analytical one.

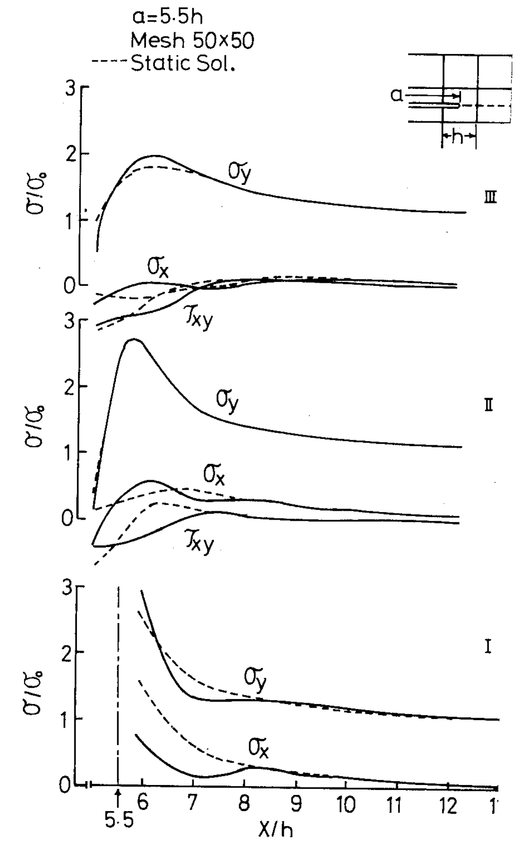

Fig. 2 Stress distribution around a crack tip in steady state

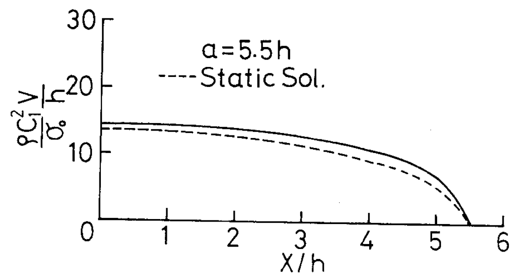

Fig. 3 Configuration of crack opening displacement of a crack in steady state

2.2.2 *Crack extending at a constant speed*

The crack extending at a constant speed is simulated by advancing the crack tip by one mesh every specified period. It was found that a sudden release of a nodal force at the nearest point of the crack tip results in more or less fluctuating crack configuration, especially when the crack propagates at lower speeds. To avoid this fluctuation the nodal force at the nearest point of the crack tip was decreased linearly with the time which is relevant to the given crack speed.

The problem solved is a crack extending at constant speed in a square plate with the size of B=H=70h. The stress distribution along the crack line and the configuration of the crack opening displacement are shown in Figs. 4 and 5, respectively. The dashed lines are the analytical solutions for an infinite body obtained by Broberg[3]. The computed configurations of the crack opening displacement (solid

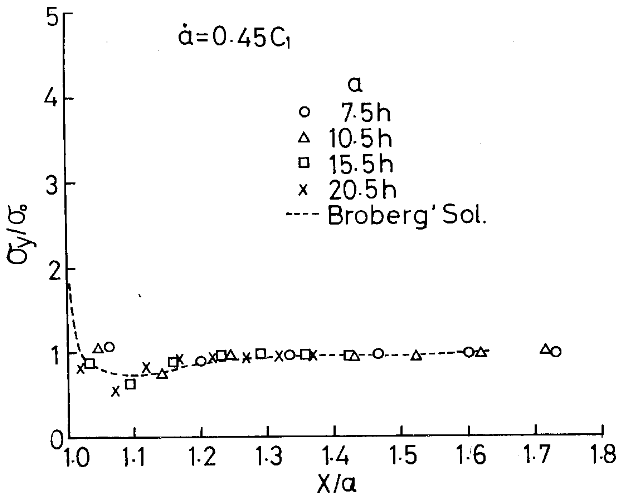

Fig. 4 Stress distribution along crack line of a crack extending at constant speed

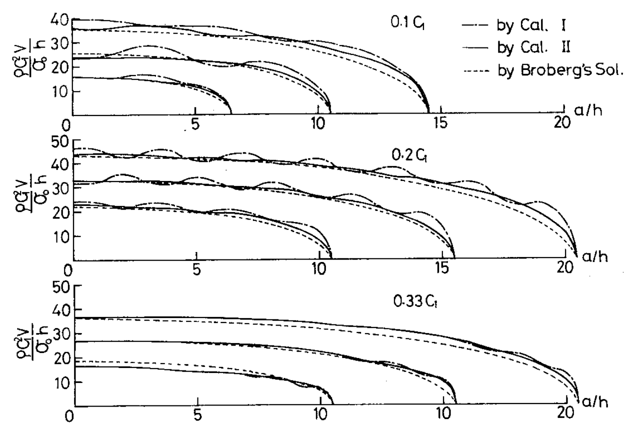

Fig. 5 Configuration of crack opening displacement of a crack extending at constant speed

line) by the improved method of releasing nodal force is found to agree better with the Brobergs' analytical one than those obtained from sudden release of nodal force.

2.2.3 *Energy*

Up to date the criteria for crack propagation and arrest are mostly discussed on the basis of considerations on energy flow into running crack tip. In order to define fracture toughness of a material against fast running crack, it is very important to know the amount of energy dissipated which will depend on crack velocity.

The law of conservation of energy is expressed as follows during crack propagation:

$$D=W-U-K \tag{7}$$

$$\Delta D=\Delta W-\Delta U-\Delta K \tag{7)'$$

where W, U, K, D and Δ are work done by external load, strain energy, kinetic energy, dissipated energy and their incremental values, respectively. The energies which can be estimated by finite difference calculations are the three terms of righthand side of eq. (7), and thus the term D can be obtained indirectly from those three which would approximately be equal to fracture energy in case of fracture under small scale yielding.

Further, to compute W, U and K respectively for a cracked body is rather complicated and besides there is some possibilities to introduce considerable numerical errors. Considering that the righthand term of Eq. (7)' is nothing but the energy available for incremental crack advance, it is equal to the energy required to close the crack by that incremental value which is so called "crack closure energy" and an extension of the technique adopted by Irwin[6] in static case. Thus we have incremental crack closure energy ΔE_c as expressed by

$$\Delta E_c=\Delta a\times\int_0^v \sigma_y(t)\ dv(t) \tag{8}$$

where $\sigma_y(t)$ and $v(t)$ are stress and displacement at the nearest point of the crack tip as functions of time, respectively. Figure 6 shows schematically the relation between

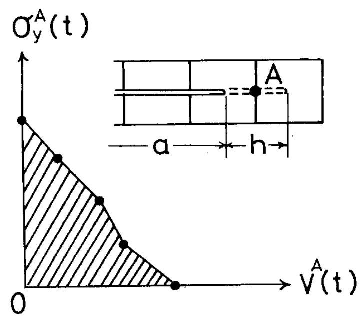

Fig. 6 Relation between stress and crack opening displacement at point A

Table 1 Mechanical properties and chemical compositions of KAS

Young's Modulus E (kg/mm^2)	Density ρ (g/cm^3)	Poisson's Ratio ν	Yield Strength σ_y (kg/mm^2)	Tensile Strength σ_u (kg/mm^2)	Elongation (%)
20180	8.0	0.298	28	43	34

Mechanical Properties of KAS

C	Si	Mn	P	S
0.11	0.33	0.75	0.022	0.008

Chemical Composition (%)

$\sigma_y(t)$ and $v(t)$. The shaded area is the work done ΔE_c during the crack extension by Δa. Figure 7 shows the variations of dissipated energy D obtained from computation of W, U and K as compared with the given speeds. The dashed line is an analytical solution obtained by Broberg[3], and E_c agree excellently with the analytical one. It is concluded that the fracture energy or dissipated energy rate dD/da can be computed more easily and accurately from crack closure energy ΔE_c than from W, U and K.

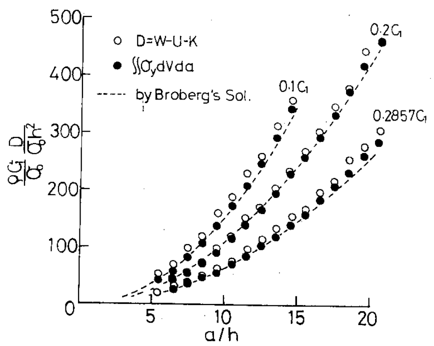

Fig. 7 Variation of dissipated energy with crack extension

3. Dynamic Fracture Characteristics of Ship Steels

An experimental investigation using a ship hull steel KAS was made to clarify the fundamental aspects of brittle crack propagation and arrest in structural steel. For the overall elastic behavior of brittle crack propagation in structural steels, it is assumed here that the associated energies except fracture energy are approximately calculated by elasticity theory as mentioned in the foregoing section and effects of shear lips and three dimensional feature of a propagating crack front are disregarded.

The brittle crack propagation tests adopted are standard size and large size Double Tension Test and DCB Test. The latter two were carried out by Mitsubishi Heavy Industries, Ltd. and Sumitomo Heavy Industries, Ltd., respectively.

The effects of specimen size and type of loading are examined from these three test series.

3.1 *Experiment*

3.1.1 *Material*

A 15 mm thick ship hull steel (NK code KAS) is used. The mechanical properties and chemical compositions of the steel are shown in Table 1.

3.1.2 *Testing procedure*

Two series of standard size Double Tension Test are carried out, i.e. flat temperature type (SP series) and gradient temperature type (SA series). In the SP series, a fast crack runs completely through the specimen width. In the SA series, on the other hand, a fast crack decelerates and is arrested because of an increase of material toughness due to temperature gradient. Figure 8 shows the specimen configuration and arrangement of crack detector gages and strain gages. The specimen consists of a crack initiation part and a 500 mm wide crack propagation part. The specimen is welded to two 30 mm thick pulling plates, and the total length between two loading pins is about 3000 mm. The welding residual stresses are mechanically relieved by pre-loading. Uniform tensile

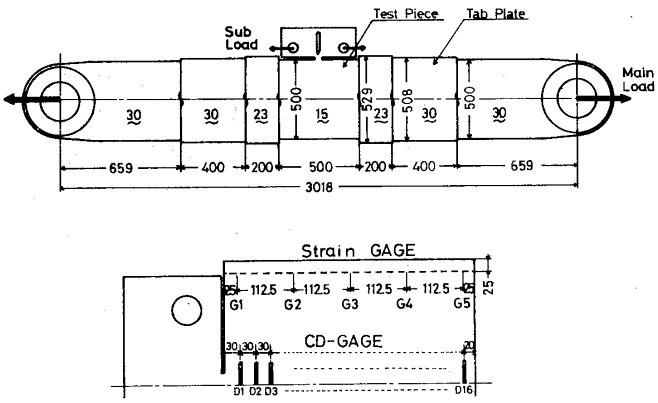

Fig. 8 Specimen configuration and arrangement of crack detector gages and strain gages

stress is applied to propagation part and a brittle crack is initiated from the supercooled initiation part by sub-load and is run into the propagation part.

The crack velocity is measured from the change in the electric resistance of crack detector gages on the propagation part at 30 mm intervals. Transient variations of the strains with the crack extension are recorded at the locations G1 to G5 shown in Fig. 8.

3.1.3 *Results of SP series*

The experimental conditions and mean velocities obtained are shown in Table 2. Four different applied stresses (12, 16, 20 and 24 kg/mm^2) are adopted to examine the influence of initial applied stress σ_0 on crack velocity. Testing temperatures are -60°C and -40°C. Figure 9 shows the variation of crack velocity. The crack seems to run at almost constant velocity during

Table 2 Experimental results of SP test series

	σ_0 (kg/mm^2)	T (°C)	Ps (TON)	$\dot{a}$ (m/s)	
SP-1	20	-61	6.5	1100	
SP-2	16	-60	25.2	–	CURVE
SP-3	24	-60	8	850	BRANCH
SP-4	16	-61	22.5	–	NO GO
SP-5	24	-40	21	–	
SP-6	20	-40	19	950	
SP-7	16	-42	23.5	900	
SP-8	12	-40	15	750	

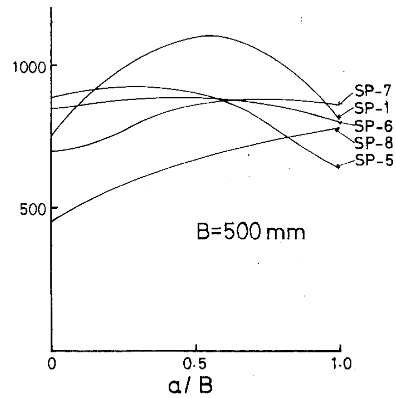

Fig. 9 Variations of crack velocity in SP series tests with crack extension

crack propagation. The maximum crack velocities obtained in each of the experiments are relatively low (about $0.2\sqrt{E/\rho}$ ≈ 1000m/s), as compared to so-called terminal velocity ($0.38\sqrt{E/\rho}\approx 1890$m/s) obtained by Roberts et al[7] also to the velocity in large size brittle crack propagation-arrest test conducted previously.

3.1.4 *Results of SA series*

In order to examine the influence of initial applied stress σ_0 on crack velocity using Type I temperature distribution shown in Fig. 10, four different applied stresses (8, 12, 16 and 20 kg/mm^2) are adopted. The experiments using Type II and III temperature distributions as shown in Fig. 10, are carried out at σ_0=16kg/mm^2

to examine the effect of temperature gradient. The experimental conditions and main results are shown in Table 3. T_A, a_A and K_c denote temperature at crack arresting point, arrested crack length and arrest toughness based on static approximation, respectively. Figure 11 shows the variations of crack velocity with crack growth. A crack running rapidly into the propagation part begins to decelerate and is shortly arrested abruptly due to the increase of material toughness with temperature.

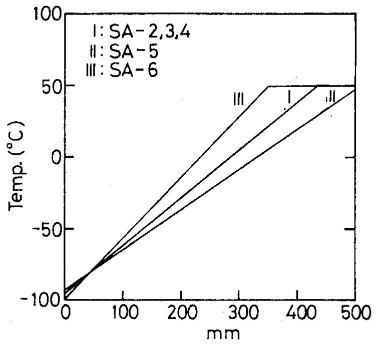

Fig. 10 Temperature distribution for SA series specimen

Table 3 Experimental results of SA test series

	σ_0 (kg/mm^2)	Ps (TON)	T_A (°C)	$\dot{a}_A$ (mm)	Kc (kg/mm$^{3/2}$)	$\dot{a}$ (m/s)
SA-1	8	20	—	—	—	—
SA-2	12	11	0	280	417	650
SA-3	16	7	8	305	604	750
SA-4	20	20	12	320	794	1000
SA-5	16	26	14	373	878	850
SA-6	16	12.5	4	241	492	750

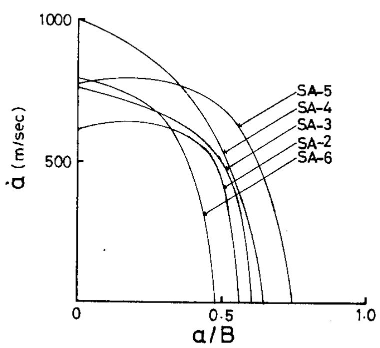

Fig. 11 Variations of crack velocity in SA series tests

3.2 *Analysis and Discussion*

3.2.1 *Dynamic fracture mechanics analysis with the use of finite difference method*

The equations of motion for two dimensional elastic body are solved numerically with the experimentally obtained time dependent boundary conditions. The dilatational wave velocity C_1 and distortional wave velocity C_2 are about 5670 m/s and 3100 m/s, respectively. Overall domain including pulling plates are subjected to numerical analysis. Mesh size h and time increment Δt adopted are 10 mm and 1 μ sec ($C_1\Delta t/h$ =0.567), respectively and the explicit method is used in analysis. Because the exact boundary condition at grips is not known, analyses are made under both fixed load and fixed grip conditions.

Assuming that the term D in eq. (7) is mostly the energy dissipated in the fractuared surface layers dynamic fracture toughness K_D is defined as follows by the analogy with static case.

$$K_D=\sqrt{\frac{E}{1-\nu^2}\frac{dD}{da}} \tag{9}$$

When estimating K_D using eqs. (7) and (9), however, the amount of D sometimes becomes very small as compared to U and/or W, that is the order of 10^{-2} to 10^{-3} times as small as U or W, and thus an accurate estimation of D can not be expected because of inevitable numerical error in the numerical technique. As described in 2, an alternative to compute the dissipated energy rate is provided by considering crack closure energy ΔE_c . Then K_D is defined in terms of ΔE_c as follows:

$$K_D=\sqrt{\frac{E}{1-\nu^2}\frac{\Delta E_c}{h}}=\sqrt{\frac{E}{1-\nu^2}\int\sigma_y(t)\,\{dv(t)\}} \tag{10}$$

3.2.2 *Strain distribution*

Figure 12 shows an example of the comparison between measured and computed variation of strain distribution during crack propagation. The ordinate indicates the change in strain from its initial value ϵ_0. The numerals in the figure represent the time elapsed after trigger is stared. Although computed strains show small irregular fluctuation, general trend of computed strain distribution agrees relatively well with those obtained from the experiment.

The results of analysis under fixed grip condition does not differ from those under fixed load condition at all. This may be attributed to the fact that the fast crack ran through the specimen or was arrested before the stress wave reflected from

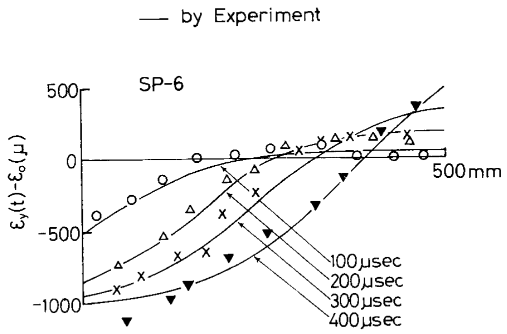

Fig. 12 Comparison between measured and computed variation of strain distribution during crack propagation

specimen outer boundary came to the boundary concerned. But, as shown in Fig. 13, the difference between the two loading conditions becomes evident after about 520 μsec required for the reflected stress waves to arrive at crack propagation line. This figure shows computed strain distributions for both conditions at 700 μsecond in SA series after a crack enters into the propagation part. Judging from Fig. 13, the experimented boundary condition lies between fixed grip (solid mark) and fixed load condition (open mark) and the influence of boundary condition is found to be negligible if crack propagation and arrest are finished before arrival of reflected stress waves. Therefore, only the results of the solution under fixed grip condition will be referred to hereinafter.

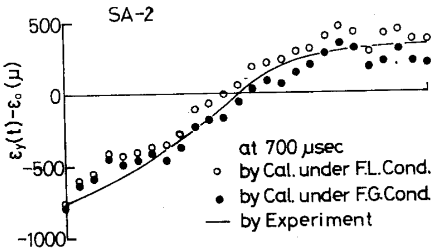

Fig. 13 Comparison between measured and computed variation of strain distribution during crack propagation

3.2.3 *Energy changes and dynamic fracture toughness K_D*

Figures 14(a) and (b) show energy changes due to crack extension under fixed grip condition in SP and SA series, respectively. Static strain energy changes are also shown in these figures for reference. It is generally observed that part of U decreased with crack extension is transformed into kinetic energy K and dissipated energy D and thus both K and D increase. It is natural that the decrease of U in dynamic

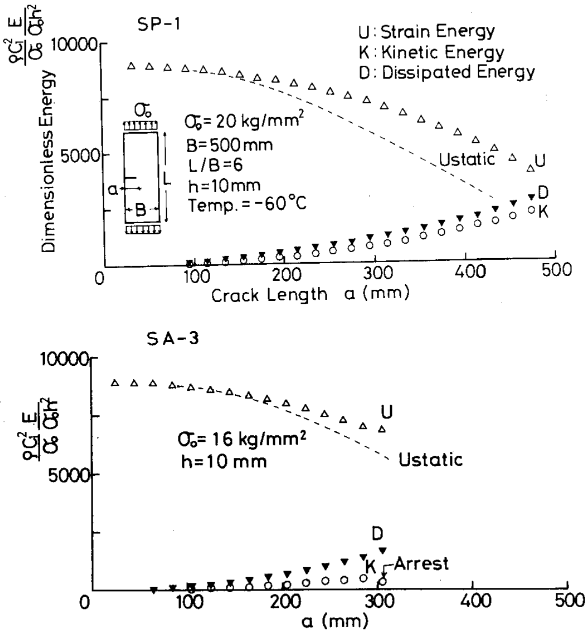

Fig. 14(a),(b) Energy changes due to crack extension case is less than those in static case and the difference of U in two cases becomes larger with the increase of crack length, because of necessity of kinetic energy for the former case. It is impossible to treat with crack propagation and arrest of large crack on the basis of static approximation for the above reasons.

Figure 15(a) and (b) show the variation of dynamic fracture toughness K_D with crack extension in SP and SA series, respectively. The variation of crack velocity and static stress intensity factor for fixed grip condition are also indicated in each figure for reference. For SA series the temperature distribution is also shown in the same figures. In SP series, a gradual increase of K_D corresponds to the variation of crack

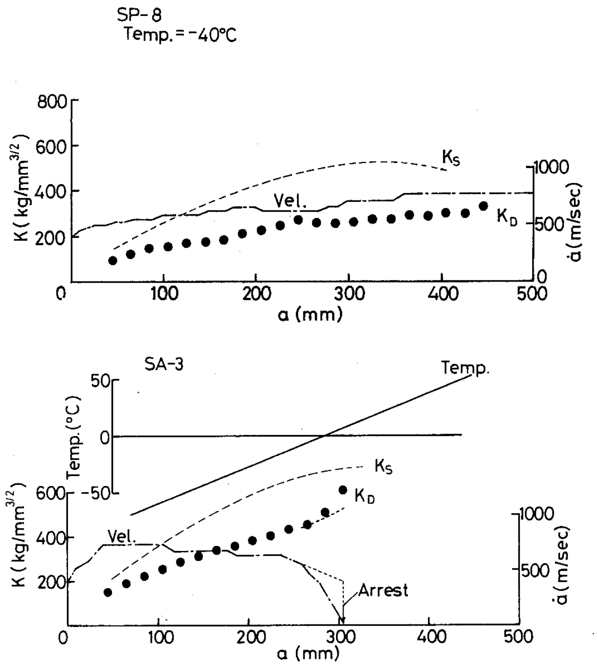

Fig. 15(a),(b) Variation of dynamic fracture toughness with crack extension

velocity. Relatively large increase of K_D with crack extension in SA series, on the other hand, corresponds not only to the linear increase of temperature but also to its crack velocity dependence such as observed in SP series. The accuracy of measurement of crack velocity is poor just before crack arrest, because of an extended plastic zone ahead of crack tip and plate thickness contraction. Therefore, two types of crack velocity pattern shown in Fig. 15(b) are input in the analysis. The dashed line in this figure is assumed to account for the existence of lower bound speed proposed by Ikeda[8]. There are some difference of K_D obtained from the above two crack velocities and K_D tends to increase and approach K_s rapidly. This shows the importance of accurate measurement of crack velocity just before it is arrested. But the values of K_D are always less than static stress intensity factor K_s during crack propagation as the case with SP series. This is to be noted comparing with the situations in DCB test to be mentioned later.

3.2.4 *Results of large size double tension test*

Wide plate double tension test denoted SI series in this paper has been conducted[9] using the same material at Nagasaki Technical Laboratory, Mitsubishi Heavy Industry Ltd. The results of two testings where cracks were arrested are subjected to the present analysis. Figure 16 shows the energy changes due to crack extension for the modeled test specimen ($1600B \times 6000L \times 15t$ mm). Spatial mesh size h is 30 mm. Figure 17 shows the variation of K_D with crack extension. The static stress intensity factor K_s under fixed grip condition, the variation of crack velocity

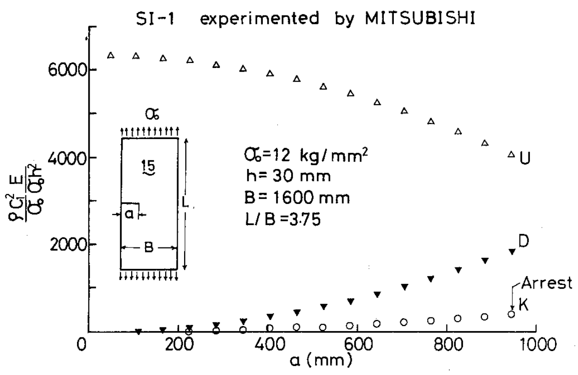

Fig. 16 Energy changes due to crack extension

and temperature distribution are also shown. The crack velocity is almost constant during crack propagation in these tests and thus the increase of K_D is regarded as corresponding due to temperature gradient.

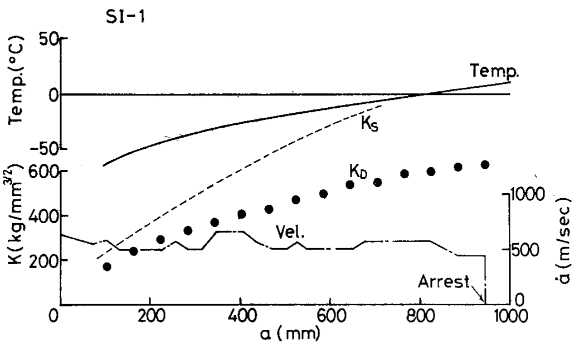

Fig. 17 Variation of dynamic fracture toughness with crack extension

3.2.5 *Results of DCB test*

Experiment using DCB (Double Cantilever Beam) specimen made of the same material was carried out by Sumitomo Heavy Industries Ltd.[9]. Some of the results are now analyzed using a beam on elastic foundation model[10] for simple dynamic fracture mechanics analysis. The DCB test specimen configuration and the one dimensional model are shown in Fig. 18 and the specimen dimensions are $100H \times 530L \times 15b$ (mm).

The equations of motion for the beam on elastic foundation model of the DCB specimen have their origin in the theory of elasticity. They are obtained by exploiting simplification suggested by the beam-like character of the DCB specimen which result in equations similar to those for the Timoshenko beam. In this model the arms of the DCB specimen are assumed to be Timoshenko beams with lateral and rotational inertia. To simulate a moving crack, each spring or the elastic foundation is systematically removed.

The governing equations for the model of the DCB specimen can be written as

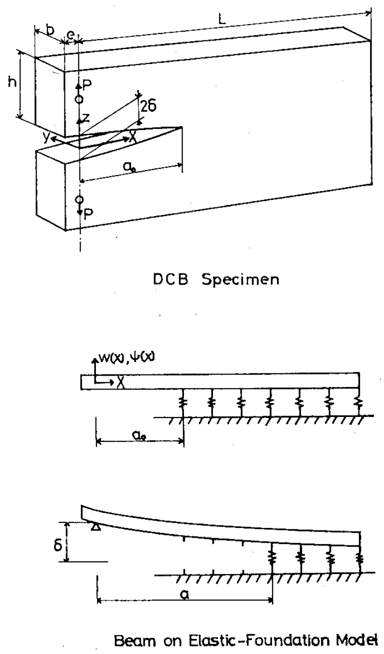

Fig. 18 (a),(b) Configuration of DCB specimen and beam on elastic foundation model

$$EI\frac{\partial^2\Psi}{\partial x^2}+\kappa GA\left(\frac{\partial w}{\partial x}-\Psi\right)-H^*K_r\Psi=\rho I\frac{\partial^2\Psi}{\partial t^2}$$

$$\kappa GA\left(\frac{\partial^2 w}{\partial x^2}-\frac{\partial\Psi}{\partial x}\right)-H^*K_e w=\rho A\frac{\partial^2 w}{\partial t^2} \qquad (11)$$

where

w = average deflection of the cross section
Ψ = mean angle of rotation of the cross section about the neutral axis
I = moment of inertia $(=bH^3/12)$
A = area of the cross section
G = shear modulus $(=\frac{E}{2(1+\nu)})$
K_e = extentional stiffness of the foundation $(=2Eb/H)$
K_r = rotational stiffness of the foundation $(=\kappa GA/2)$
κ = shear-deflection coefficient of the beam $(=10(1+\nu)/(12+11\nu))$
H^* = modified Heavisible step function

The strain energy U and the kinetic energy K of the system can be expressed as follows.

$$U=\int_{-e}^{L}\left\{EI\left(\frac{\partial \Psi}{\partial x}\right)^{2}+\kappa GA\left(\frac{\partial w}{\partial x}-\Psi\right)^{2}+H^{*}(K_{e}w^{2}+K_{r}\Psi^{2})\right\}dx$$

$$K=\int_{-e}^{L}\left\{\rho A\left(\frac{\partial w}{\partial t}\right)^{2}+\rho I\left(\frac{\partial \Psi}{\partial t}\right)^{2}\right\}dx \qquad (12)$$

The specimen is slowly loaded by forcing a split wedge between pins. Since the wedge loading is inherently stiff, crack extension proceeds with essentially constant displacement at the load point. Under this condition, external work is zero. Consequently,

$$\frac{dD}{da}=-\frac{dU}{da}-\frac{dK}{da} \qquad (13)$$

By substituting Eq. (12) into Eq. (13), dynamic fracture toughness K_D can be written as

$$K_{D}=\sqrt{\frac{E}{1-\nu^{2}}\{K_{e}w^{2}(a)+K_{r}\Psi^{2}(a)\}} \qquad (14)$$

where the bracketed term represents the elastic strain energy of the foundation element just at the crack tip.

Three experimental results at the temperature of -40°C are analyzed using the finite difference method (FDM). The mesh sizes in the FDM calculation are

$\Delta x=5$ mm

$\Delta t=0.7\ \mu$sec

As example of calculation results, Fig. 19(a) and (b) show the variation of dynamic material toughness K_D and change rates of strain and kinetic energies with crack extension. In the case of Double-Tension Test, K_D is always smaller than K_s and the kinetic energy K increases continuously during crack extension. In this case, during the first stage of extension K_D is smaller than K_s and kinetic energy K increases, but during the latter stage K_D is larger than K_s and K decreases. It seems that the differences between the two cases depend on the difference of the loading condition and the specimen configuration.

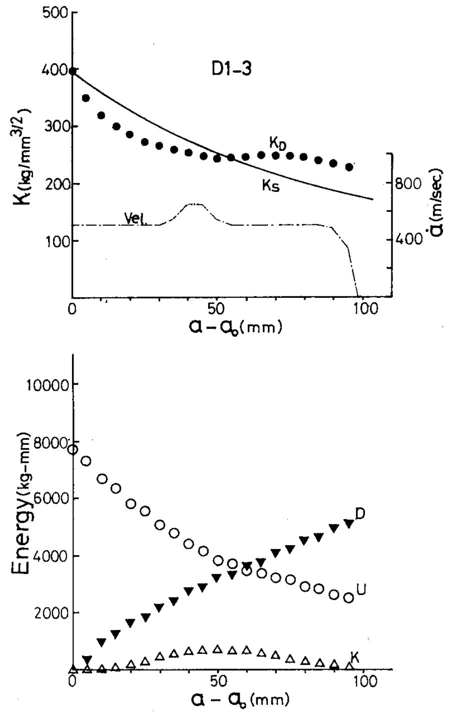

Fig. 19(a),(b) Variation of dynamic fracture toughness and energies with crack extension in DCB specimen

Perhaps the most important result in this section is that for the DCB specimen the kinetic energy is almost completely recovered until the crack is arrested. Namely the kinetic energy provides a very significant contribution to maintaining unstable crack extension and dynamic consideration is indispensable.

3.2.6 *Material toughness characterization*

The material toughness for fast crack propagation is to be specially characterized by putting together the results of three different types of brittle crack propagation arrest test. As discussed before, the material toughness is regarded as governed by two primary parameters, i.e. crack velocity $\dot{a}$ and temperature T, and is expressed by

$$K_{D}=f(\dot{a},\ T) \qquad (15)$$

The relation between K_D and crack velocity $\dot{a}$ is obtained from the three types of brittle crack propagation-arrest test for the temperature of $-40°C$ as shown in Fig. 20. Despite there is a little scatter, it may be concluded that K_D is defined as a specific function of crack velocity for a given temperature, and it is an intrinsic material characteristic curve independent of specimen configuration. Figure 21 shows the relations between K_D and crack velocity for various temperatures estimated mainly from the results of SA series tests. The similar relation between K_D and crack velocity as in Fig. 20 exists for a given temperature. Figures 20 and 21 justify the validity of the expression of eq. (15).

Figure 22 shows the relation between toughness value at crack arrest K_D^A obtained from FDM computation and temperature. Open mark indicates arrest toughness K_c based on static approximation. Symbol bar I in this figure shows the range of the values obtained from previously mentioned two crack velocity inputs. Mark ◇ represents K_D^A in SI series (large size Double Tension Test). K_D^A does not seem to be much different from K_c but

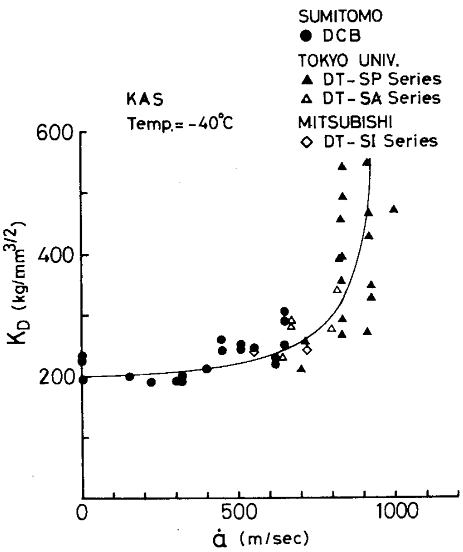

Fig. 20 Dynamic fracture toughness of KAS as a function of crack velocity for the temperature of $-40°C$

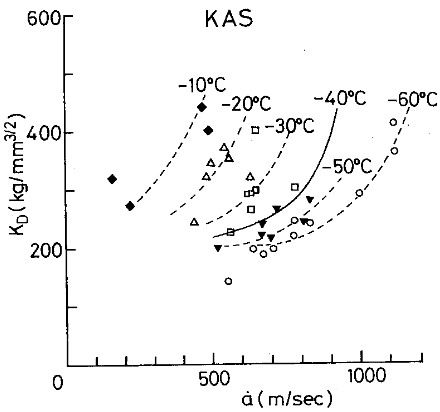

Fig. 21 Dynamic fracture toughness of KAS as a function of crack velocity for various temperatures

K_D^A depends on all the processes preceding crack arrest. On the other hand, K_c means static stress intensity factor at the point of crack arrest. It is evident from Fig. 22 that material arrest toughness obtained from dynamic analysis can not be approximated by static counterpart in general and also that experimentally proven inconsistency between very wide plate test and standard size test comes from the disregard for dynamic effect.

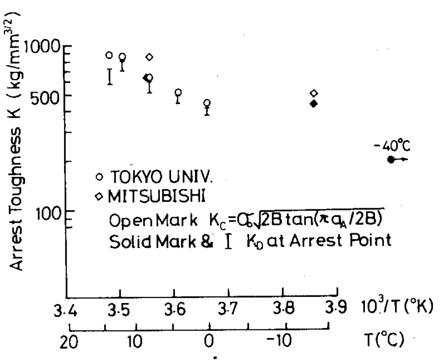

Fig. 22 Dynamic arrest toughness vs. temperature

3.2.7 *Preliminary approach to prediction of fast crack propagation and arrest*

Once the material toughness as expressed by eq. (15) is known, the behavior of a fast crack will be predicted by solving the governing equation of motion for the crack expressed by

$$G_d = G_D(\dot{a}, T) \tag{16}$$

where G_d is crack driving force which depends on crack size, crack velocity, and possibly other geometrical and mechanical boundary conditions and G_D is dynamic energy release rate. But analytical expression for G_d has been available only for simple limited cases. In general it is difficult to solve eq. (16) without resource to numerical technique.

In the following a preliminary consideration for crack arrester design will be made with the use of the experimentally obtained K_D for a simple crack.

When a crack propagates in an infinite plate subjected to uniform tensile stress σ, dynamic stress intensity factor K_d is given by Freud[11] as

$$K_d(a, \dot{a})=k(\dot{a})K_S(a) \tag{17}$$

where K_s is static stress intensity factor and a universal function of crack speed $k(\dot{a})$ which decreases monotonically with $\dot{a}$ from unity at zero crack speed to zero at the Rayleigh wave velocity C_R. The relation between dynamic energy release rate G_D and dynamic stress intensity factor K_d is given as[11]

$$G_D(a, \dot{a})=\frac{1-\nu^2}{E}A(\dot{a})K_d^2(a, \dot{a}) \tag{18}$$

where $A(\dot{a})$ is monotonically increasing function with $\dot{a}$ and is unity at zero crack speed and becomes unbounded at the Rayleigh wave velocity C_R. From the conservation of energy the following equation is derived from eqs. (9), (17) and (18).

$$k^2(\dot{a})A(\dot{a})K_S^2=K_D^2(\dot{a}, T) \tag{19}$$

As $k^2(\dot{a})\ A(\dot{a})$ can be approximated by a simple function[12], eq. (19) becomes as follows.

$$\sqrt{1-\frac{\dot{a}}{C_R}}K_S=K_D(\dot{a}, T) \tag{20}$$

The lefthand and righthand terms of eq. (20) correspond to crack driving force and material resistance, respectively. This equation gives crack velocity for a given crack length and temperature for a propagating crack in a plate which is so large that the crack never encounter the effect of reflected stress wave from boundary.

Figure 23(a) and (b) shows the comparison between measured and calculated velocity in Double Tension Test, which is obtained by solving eq. (20) using the toughness curve shown in Fig. 21. The calculated variation of crack velocity and crack arrest length agree well with experimental one. This is because a crack propagates through the specimen or arrests until an arrival of reflected stress wave from boundary to crack tip, in other words, this specimen may be regarded as an infinite body in this sense. The result of applying eq. (20) to DCB test is shown in Fig. 24.

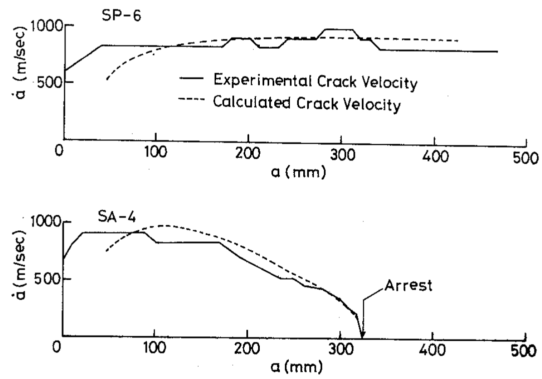

Fig. 23(a),(b) Comparison between measured and calculated velocity

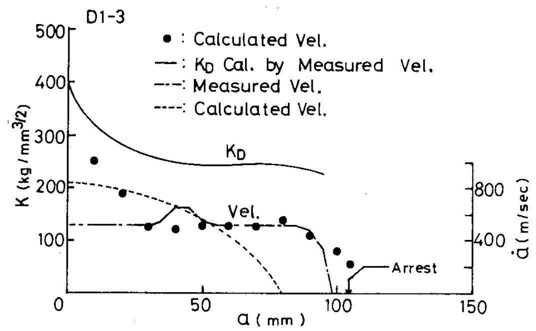

Fig. 24 Comparison between measured and calculated velocity in DCB specimen

As reflected stress wave from boundary affects remarkably a propagating crack in DCB test, such a specimen cannot be treated as an infinite body and then calculated velocity (dashed line) by eqs. (15) and (20) is quite different from measured one. On the other hand, calculated velocity (solid mark) by eqs. (14) and (15) using above-mentioned beam model agrees very well with measured one. As discussed previously, almost all the kinetic energy is eventually transformed into crack driving energy in DCB specimen which is affected by considerable amount of reflection of stress waves.

A crack in an infinite plate as governed by eq. (20) and a crack in DCB specimen are the two extreme cases in terms of the amount of contribution of kinetic energy to driving the crack.

The real structures lie between the above two extremes. Therefore, a simple approach will be possible by appropriately defining the amount of contribution of kinetic energy taking due account to the characteristic features of structural element under consideration. In order to establish an arrest design for steel structure, it will further be necessary to collect data of clearly defined material toughness and to develop some practical simplification to such an approach which avoids the necessity of complicated dynamic analysis.

4. Concluding Remarks

The fundamental aspects of brittle crack propagation and arrest in structural steels have been considered primarily from the energetic point of view for the final goal of establishing a relevant crack arrester design methodology. Dynamic fracture mechanics analysis was made using finite difference method on brittle fracture propagation-arrest test using a ship steel. Despite the numerical analysis used is an approximation without non-based on linear theory of elasticity, it is found that dynamic consideration is indispensable for general interpretation of fast fracture and crack arrest and material toughness can be defined as a function of temperature and crack velocity.

Using the experimentally obtained toughness, crack propagating behavior is successfully predicted in case where no kinetic energy is recovered to drive the crack further. This approach provides an elementary method of crack arrester design. Further works are needed to define quantitatively the material properties associated with fast fracture and to establish a general and relevant methodology for designing crack arrester in various types of structures.

Reference

1) E.H. YOFFE ; The Moving Griffith Crack, Phil. Mag., Vol. 42, p. 739 (1951)
2) J.W. CRAGGS ; On the Propagation of a Crack in an Elastic-Brittle Material, J. Mech. Phys. Solids, Vol. 8, pp. 66-75 (1960)
3) K.B.BROBERG ; The Propagation of a Brittle Crack, Ark. Fys., p. 546 (1960)
4) M. SHMUELY and D. PERETZ ; Static and Dynamic Analysis of the DCB Problem in Fracture Mechanics, Int. J. Solids and Structure, Vol. 12, pp. 67-79 (1976)
5) A.W. MAUE ; Die Entspannungswelle bei plötzlichem Einschnitt enines gespanntern elastischen Körpers, Z. Angew. Math. Mech., Bd. 34, Nr. 1/2, pp. 1-12 (1954)
6) G.R. IRWIN ; Handbuch der Physik, Vol. 6, p. 551 (Berlin, 1958)
7) D.K. ROBERTS and A.A. WELLS ; The Velocity of Brittle Fracture, Engineering, Vol. 178, pp. 820-821 (1954)
8) Y. AKITA and K. IKEDA ; On the Brittle Crack Propagation and Arrest with Special Reference to ESSO Test with Temperature Gradient, Journal of the Society of Naval Architects of Japan, Vol. 112, pp. 153-162 (1962) (in Japanese)

9) "Study on Fracture Control Design in Ship Structure", Report No. 297, Shipbuilding Research Association of Japan (1978) (in Japanese)
10) "Fast Fracture Resistance and Crack Arrest in Structural Steel", SSC-242 Progress Report, Ship Structure Committee (1973)
11) L.B. FREUND; Crack Propagation in an Elastic Solid subjected to General Loading-I Constant Rate to Extension, J. Mech. Phys. Solids, Vol. 20, pp. 129-140 (1972)
12) "A Study of Ship Hull Crack Arrester Systems", Final Technical Report on Project SR-226, Ship Structure Committee (1976)